OATAO

Open Archive Toulouse Archive Ouverte

Open Archive TOULOUSE Archive Ouverte (OATAO)

OATAO is an open access repository that collects the work of Toulouse researchers and makes it freely available over the web where possible.

This is an author-deposited version published in : http://oatao.univ-toulouse.fr/
Eprints ID : 13979

To cite this version : Lallemant, Lucile and Roussel, Nicolas and Fantozzi, Gilbert and Garnier, Vincent and Bonnefont, Guillaume and Douillard, Thierry and Durand, Bernard and Guillemet-Fritsch, Sophie and Chane-Ching, Jean-Yves and Garcia-Gutierez, Domingo and Aguilar-Garib, Juan *Effect of amount of doping agent on sintering, microstructure and optical properties of Zr- and La-doped alumina sintered by SPS.* (2014) Journal of the European Ceramic Society, vol. 34 (n° 5). pp. 1279-1288. ISSN 0955-2219

Any correspondance concerning this service should be sent to the repository administrator: staff-oatao@listes-diff.inp-toulouse.fr

Effect of amount of doping agent on sintering, microstructure and optical properties of Zr- and La-doped alumina sintered by SPS

Lucile Lallemant [a,b], Nicolas Roussel [c], Gilbert Fantozzi [a,b], Vincent Garnier [a,b,*],
Guillaume Bonnefont [a,b], Thierry Douillard [a,b], Bernard Durand [c], Sophie Guillemet-Fritsch [c],
Jean-Yves Chane-Ching [c], Domingo Garcia-Gutierez [d], Juan Aguilar-Garib [d]

[a] *Université de Lyon, CNRS, France*
[b] *Insa-Lyon, MATEIS UMR5510, F-69621 Villeurbanne, France*
[c] *Université de Toulouse, CNRS-UPS-INPT, CIRIMAT, 118 route de Narbonne, 31062 Toulouse, France*
[d] *Centro de Innovacion, Investigacion y Desarrollo en Ingeniera y Tecnologica, UANL, Carretera al Aeropuerto, Apodaca, Nuevo Leon, Mexico*

Abstract

SPS-produced α-alumina samples are prepared from powders doped with different amounts of Zr^{4+} and La^{3+} cations. Zr^{4+} cations segregate at grain boundaries. m-ZrO_2 particles are formed at 570 but not at 280 cat ppm. A β-alumina $LaAl_{11}O_{18}$ structure is found at 310 cat ppm when the lanthanum grain boundary solubility limit is exceeded ($\sim$200 cat ppm). 100 cat ppm La is sufficient to block the diffusion path across grain boundaries and inhibit grain growth. Both doping cations disturb the grain boundary diffusion whatever their amount. They delay the densification at higher temperatures while limiting grain growth. The real in-line transmittance (RIT) of α-alumina is improved due to the reduced grain size. Nevertheless, increasing the cation amount leads to an increase in porosity or even the formation of secondary phase particles, both detrimental for optical properties. Finally, optimised amounts of cation of 200 and 150 cat ppm are found for La- and Zr-doped alumina, respectively.

Keywords: Al_2O_3; Doping; Spark plasma sintering; Grain sizes; Optical properties

1. Introduction

Properties of ceramic materials are governed by their microstructure. Therefore, the best microstructure suitable for a given application should be obtained after sintering. Grain boundaries are known to play a significant role on the microstructure formation during densification and grain growth. In the case of alumina, doping cations with a larger ionic size than Al^{3+} (for example Y^{3+}, La^{3+}, Mg^{2+}) may be added to the powder before sintering. They show a strong tendency to either form a solid solution with the alumina or segregate at grain boundaries. Mass transport in the grain boundary plane and grain boundary mobility is therefore modified.[1–5] As a result, the densification can either be improved or hindered due to a higher or lower diffusivity at grain boundaries.[3] Moreover, the grain size is generally finer after sintering with such doping agents due to lower grain boundary mobility.[3,6,7] Those doping elements have been successfully used to obtain transparent polycrystalline alumina (PCA).[7–12] Indeed, because of the birefringent nature of PCA, a fine microstructure is required after sintering[13] as demonstrated by the model developed by Apetz et al. (Eqs. (1) and (2)).

$$RIT = \frac{I_2}{I_1} = (1 - R_S \cdot \exp(-\gamma_{tot} \cdot D)) \tag{1}$$

$$\gamma_{tot} = \gamma_G + \gamma_p = \frac{3\pi^2 r \Delta n^2}{\lambda_0^2} + \frac{p}{}$$

* Corresponding author at: Insa-Lyon, MATEIS UMR5510, F-69621 Villeurbanne, France. Tel.: +33 472438498.

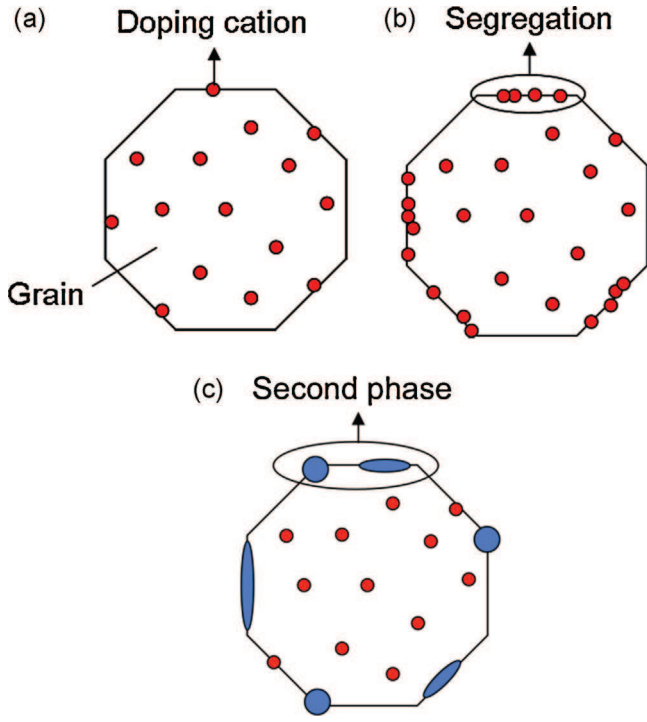*E-mail address:* vincent.garnier@insa-lyon.fr (V. Garnier).

Fig. 1. Schematic drawing of (a) solid solution, (b) grain boundary segregation, and (c) secondary phase (blue) formation. (For interpretation of the references to color in this figure legend, the reader is referred to the web version of the article.)

the average refractive index change between two adjacent grains (=0.005 for PCA), λ_0 the wavelength of the incident light beam in vacuum; p the total porosity, r_p the average pore radius and $C_{sca,p}$ the scattering cross-section of one spherical pore. Stuer et al.[14] recently showed that even if a high degree of porosity is present in the sample, there is little effect on the RIT below a critical pore size of about 50 nm. The porosity effect could thus be overestimated. Concerning the grain boundary effect, with experiments the model has shown good correlation for grain size between 300 nm and 3 μm for $\lambda = 640$ nm.[15] Nevertheless, this model does not consider a possible correlation between grain boundary scattering and grain orientation.[16] However, Cho et al.[17] have observed no significant grain boundary misorientation on alumina samples doped with 100 cat ppm Zr and 500 cat ppm La compared with pure samples. It has therefore been decided to compare our results with the Apetz model. In the literature, the role of one particular doping element on densification and grain growth of PCA is generally observed for one single quantity of this element. Nevertheless, the location of doping cations may change depending on their amount, resulting in different sintering behaviour and so different microstructures and associated properties:

(A) When the amount of doping agent is below the bulk solubility limit, doping cations are in *solid solution* homogeneously distributed within the grain (Fig. 1(a)). However, this case usually does not happen as bulk solubility limits are very low (a few hundred ppm[4]) depending on the doping agent ionic radii or charges.

(B) When the amount of doping agent is higher than the bulk solubility limit and lower than the grain boundary solubility limit, the additional cations *segregate* within a few nanometres[18] at the grain boundaries (Fig. 1(b)). The atomic structural environment around the segregated doping cations is similar to that it would have in known secondary phases.[4,19] Moreover, it should be highlighted that, on the one hand, the grain boundary solubility is surface dependent i.e. it depends on the grain size where finer grains will accommodate a larger amount of doping agent due to their larger surface area. On the other hand, the grain boundary solubility is also dependent on the grain boundary plane orientation,[4] resulting in a heterogeneous distribution of the segregating areas along the grain boundaries.

(C) When the doping agent amount exceeds the grain boundary solubility limit, *secondary phases* appear at grain boundaries and at triple points along with a lattice discontinuity between the alumina and the secondary phases (Fig. 1(c)).

Depending on its characteristics (ionic radius, charge, etc.), the doping element may be in solid solution, segregate at grain boundaries or form secondary phases. These phases are one of the possible light scattering sources in PCA. Their scattering coefficient can be described by Eq. (3)[9] and is added to the total scattering coefficient γ_{tot} in Eq. (2).

$$\gamma_{dop} = \frac{\langle ppmw \rangle_{dop} \cdot \rho_{Al_2O_3}}{4/3 \cdot \Pi \cdot r_{dop}^3 \cdot \rho_{dop}} \cdot C_{sca,dop} \tag{3}$$

where γ_{dop} is the light scattering coefficient by secondary phase particles; $\langle ppmw \rangle_{dop}$ the amount of doping agent in weight ppm; $\rho_{Al_2O_3}$ the theoretical density of α-Al_2O_3; r_{dop} the average radius of secondary phase particles; ρ_{dop} the theoretical density of secondary phase particles and $C_{sca,dop}$ the scattering cross-section of one spherical secondary phase particle. Thus, the formation of secondary phase particles should be avoided in order to improve optical properties, unless they are homogeneously distributed along the grain boundaries with a low size and a refractive index very close to that of PCA. In the present study, the effect of doping agent amount on the microstructure and optical properties of Zr- and La-doped alumina sintered by Spark Plasma Sintering (SPS) will be determined. Both Zr^{4+} and La^{3+} cations are larger than Al^{3+} cations: their ionic radii are 0.72 Å and 1.03 Å, respectively for 6-fold coordination compared to 0.53 Å for Al^{3+} for the same coordination number.[20] Zr^{4+} was found to be insoluble in an α-alumina lattice[21] and the bulk solubility of La^{3+} is really low (~80 cat ppm[22]) or even lower.[4] Those doping agents therefore have a strong tendency to segregate at grain boundaries. They thus limit grain growth during sintering[17,23] and improve the optical properties of alumina samples. Nevertheless, as far as we know, no study has yet been performed to highlight the role of the quantity of doping agent. The present study aims to correlate the densification behaviour, grain size after sintering and optical properties with the amount and location of La and Zr cations within an alumina matrix. In addition, optimisation of the amount of doping agent regarding the optical properties of alumina samples will be performed.

Table 1
ICP measurements on doped alumina powders after freeze-drying. AP: pure alumina, AZ: alumina and zirconium, AL: alumina and lanthanum.

Sample	Introduced doping agent amount (cat ppm)	Measured doping agent amount after freeze-drying (cat ppm)	Ratio (measured/introduced) doping agent amount
AP	0	–	–
Zr-doped alumina			
AZ150	250	150	0.6
AZ280	500	280	0.6
AZ570	1000	570	0.6
La-doped alumina			
AL40	60	40	0.7
AL100	150	100	0.7
AL200	300	200	0.7
AL310	500	310	0.6
AL670	1000	670	0.7

2. Materials and methods

The starting material was a commercial (BA15psh, Baïkowski) high purity α-Al_2O_3 aqueous slurry (solid content 73.5 wt%) with an average particle size D_{50}^{v} of 160 nm (measured by laser diffraction). The total impurity was less than 0.01 wt% (14 ppm Na, 60 ppm K, 7.1 ppm Fe, 13 ppm Si, 4 ppm Ca) as quoted by the manufacturer. The doping agents were introduced by weighing out the required amount of high purity (>99.99%) water-soluble chloride salts (Sigma–Aldrich, Germany) of zirconium ($ZrOCl_2$, $8H_2O$) and lanthanum ($LaCl_3$, $7H_2O$), adding them to the alumina slurry and mixing for 24 h by rotation of the container. The slurry was frozen in liquid nitrogen then freeze-dried for approximately 48 h at −40 °C under 0.1 mbar (Freeze-dryer: Christ Alpha 2–4) to obtain a powder. This was then sieved at 500 μm. The amounts of doping agent (cationic ratio [doping element^{X+}]/[Al^{3+}]) introduced were 250, 500, 1000 cat ppm for zirconium and 60, 150, 300, 500, 1000 cat ppm for lanthanum. Inductively Coupled Plasma (ICP) measurements (Horiba Jobain Yvon Activa) were performed to characterise the real amount of doping agent still present in the powder after freeze-drying and sieving (see Table 1).

As can be seen from Table 1, a constant ratio of doping cations is eliminated during the drying step. This suggests an equilibrium between the doping cations present at the surface of alumina particles and those present within the slurry. All amounts of doping agent given hereafter will refer to those measured by ICP after freeze-drying.

The freeze-dried powders were sintered by SPS (HP D 25/1, FCT System, Rauenstein, Germany) without any thermal pre-treatment. Indeed, this avoids large agglomerates within the powder before densification.[11] The sintering cycle was previously optimised to obtain pure transparent PCA samples.[11,24] It includes a uni-axial pressure of 80 MPa applied throughout the cycle, rapid heating to 800 °C, a heating rate of 10 °C/min from 800 °C to 1100 °C followed by slower heating (1 °C/min) up to
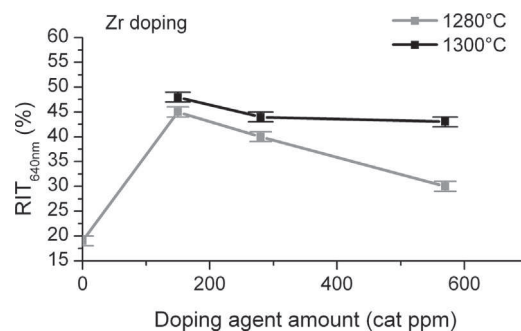

Fig. 2. RITs$_{640nm}$ of Zr-doped alumina samples sintered at T_f = 1280 °C and 1300 °C for different amounts of doping agent.

the final sintering temperature (T_f) in order to remove the residual porosity.[11,24–26] Rapid cooling ends the cycle, interrupted by a 10-min period at 1000 °C to release the residual stresses.[25,26] The final sintering temperature was optimised for each kind of doped sample in the range of 1230–1330 °C in order to obtain the best optical properties. The sintering temperature was measured 3 mm from the sample with an optical pyrometer focused on the non-through hole (3 mm diameter) of a graphite die. Then, the 20 mm diameter samples were carefully mirror-polished on both sides using diamond slurries (down to 1 μm). The transparency in the centre of the pellet (spot size = 5 mm × 2 mm) was evaluated by a RIT measurement (Jasco V-670), as it only takes into account the unscattered light through the sample (i.e. the real transmitted light). To ensure that only the RIT was measured, a shield with an appropriate aperture was placed between the sample and the detector in order to hide light scattered by more than 0.5°. For comparison purposes, all the RIT values given in this paper are evaluated for λ_0 = 640 nm and Eq. (4) allows the RIT to be obtained for the same thickness t_2 = 0.88 mm:

$$RIT(t_2) = (1 - R_S)\left(\frac{RIT(t_1)}{1 - R_S}\right)^{t_2/t_1} \qquad (4)$$

where R_S is the total normal surface reflectance (=0.14 for PCA) and $RIT(t_i)$ is the RIT for a sample thickness t_i.

An SEM ZEISS Supra55 was used to investigate the microstructure of the samples. Grain sizes were evaluated on fracture surfaces and a factor of 1.22 was applied to obtain a revised grain size.[10,13] The presence of secondary phases was determined using X-ray diffractometry (XRD Bruker D8 Advance) and their location was characterised by transmission electron microscopy (TEM) observations (TEM Titan G2 60-300 and TEM JEOL 2010F).

3. Results and discussion

3.1. Zr-doped alumina

3.1.1. Optical properties

Zr-doped powders were sintered at different T_f: 1230, 1250, 1280, 1300 and 1330 °C. The highest RITs$_{640nm}$ were obtained at T_f = 1280 and 1300 °C and these results are presented in Fig. 2.

Doping with Zr^{4+} cations enables us to increase the RIT$_{640nm}$ of alumina samples due to a reduced grain size (Fig. 3).
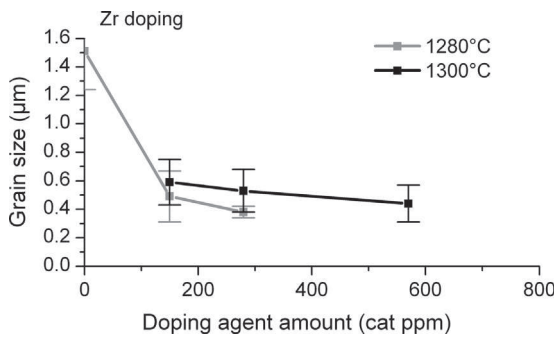
Fig. 3. Average grain sizes of Zr-doped alumina samples sintered at $T_f = 1280\,^{\circ}C$ and $1300\,^{\circ}C$ for different amounts of doping agent.

For both temperatures, the best $RITs_{640nm}$ ($45 \pm 1\%$ and $48 \pm 1\%$ for $T_f = 1280$ and $1300\,^{\circ}C$, respectively) are obtained for the lowest Zr^{4+} doping amount (AZ150). However, Fig. 3 indicates that the lower the amount of Zr^{4+} doping, the larger the grain size. For example, at $1300\,^{\circ}C$, the RIT_{640nm} decreases by about 5% between AZ150 and AZ570 whereas the grain size decreases from $0.59 \pm 0.13\,\mu m$ for AZ150 to $0.44 \pm 0.13\,\mu m$ for AZ570.

In the same way, the highest RIT_{640nm} is always obtained at $T_f = 1300\,^{\circ}C$ for a given amount of doping agent whereas the grain size is larger at this temperature. In fact, the model (Eqs. (1)–(3)) indicates that the RIT should be higher for lower grain size unless porosity or secondary phase particles are present. TEM observations are thus performed to explain the higher RIT at larger grain size.

3.1.2. TEM analysis

In a transmission electron microscope, HAADF (High Angle Annular Dark Field) images are highly sensitive to variations in the atomic number of atoms in the sample (Z-contrast images). As the atomic number of Zr ($Z = 40$) is higher than that of Al ($Z = 13$), bright contrasts in HAADF images may indicate the presence of Zr^{4+} cations within the alumina matrix. Thus, HAADF observations and EDX spectroscopy were performed on AZ570 samples sintered at $T_f = 1300\,^{\circ}C$ (Fig. 4(a)). The result indicates that no Zr^{4+} cations are located within the alumina grains. The white grain corresponds to a topological contrast. On the contrary, Zr^{4+} cations are segregated along grain boundaries as indicated by the bright contrast and EDX spectroscopy in
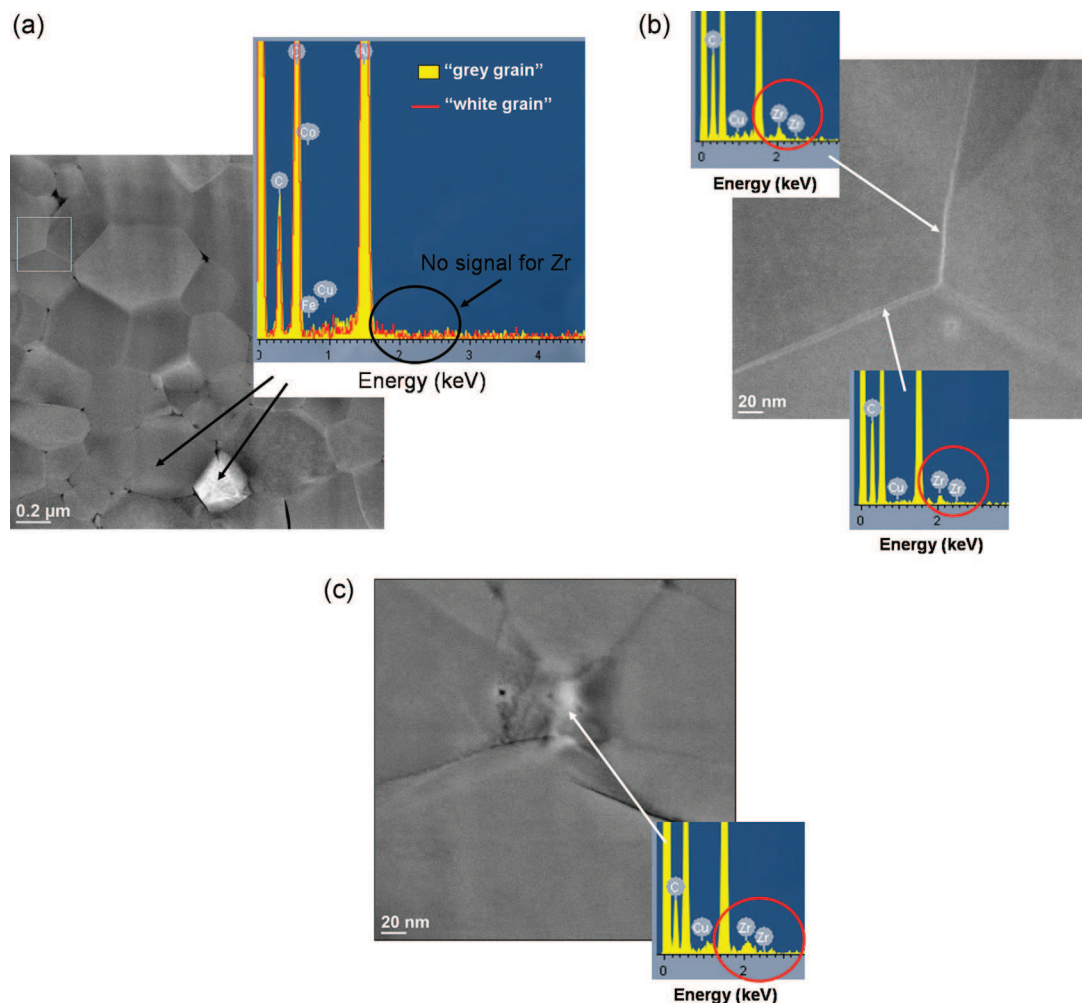

Fig. 4. HAADF observations and EDX measurements of AZ570 sample sintered at $T_f = 1300\,^{\circ}C$ (a) global view, (b) zoom of the grain boundaries, and (c) secondary phase particle observation. Bright contrasts on grain boundaries correspond to Zr^{4+} segregation. Arrows indicate the EDX analysis point.
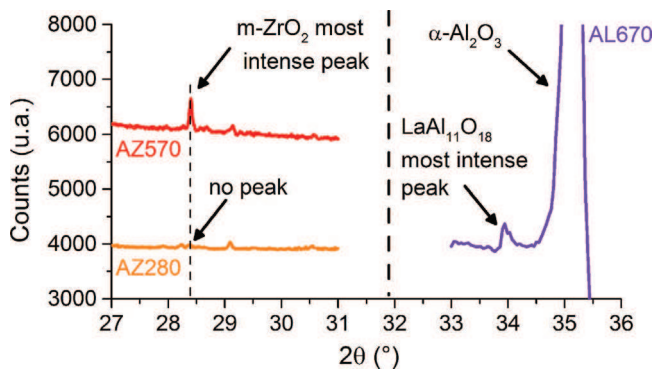
Fig. 5. XRD measurements of AZ280 (bottom left) and AZ570 (top left) samples sintered at $T_f = 1280\,°C$ and AL670 (right) sample sintered at $T_f = 1330\,°C$ (m-ZrO$_2$: ICDD 37-1484; LaAl$_{11}$O$_{18}$: ICDD 33-0699, Al$_2$O$_3$: ICDD 46-1212).
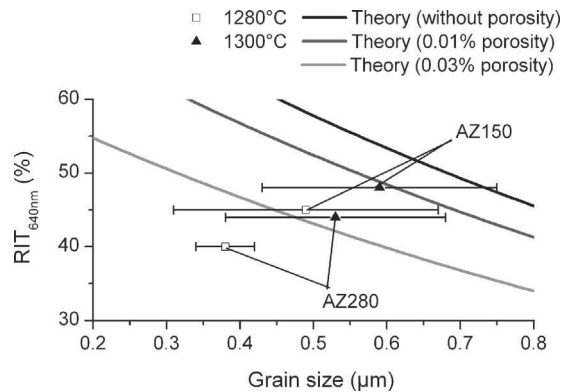

Fig. 6. Comparison of RITs$_{640nm}$ of AZ150 and AZ280 samples sintered at $T_f = 1280\,°C$ and $1300\,°C$ with theoretical models ($\lambda_0 = 640$ nm, $D = 0.88$ mm, $\phi_p = 100$ nm).

Fig. 4(b). Finally, secondary phase particles are also sometimes found at triple points (see Fig. 4(c)).

These secondary phase particles (Fig. 4(c)) are responsible for the reflection of monoclinic zirconia (m-ZrO$_2$) in XRD measurements (Fig. 5). As m-ZrO$_2$ reflection appears only on AZ570 samples (Fig. 5) and not for lower amounts of doping agent, this suggests that secondary phase particles of m-ZrO$_2$ are formed at a sufficiently high Zr concentration. For lower amounts, Zr^{4+} cations are only segregated along grain boundaries.

These results are in good agreement with a study by Wang et al.[19] who reported that for a doping agent amount of 100 cat ppm Zr, the Zr^{4+} cations segregated along grain boundaries without secondary phase formation. It is well known that Zr^{4+} cations are insoluble in an α-alumina lattice.[21] However, it is interesting to point out that the grain boundary solubility limit of Zr^{4+} cations before the formation of secondary phase particles is quite high. For grain sizes around 450 nm, this amount is thus between 280 and 570 cat ppm Zr.

Segregation of Zr^{4+} cations along grain boundaries explains why the grain size is smaller for a greater amount of doping agent (Fig. 3). Indeed, grain growth mechanisms induce diffusion across the grain boundaries. Such diffusion is hindered by the presence of impurities, such as segregated Zr^{4+} cations. Moreover, impurities lead to a solute drag phenomenon that disturbs the grain boundary mobility, all the more as the doping agent amount increases.[27] This means that grain growth will be more significant at small amounts of doping agent. For AZ570 samples, the presence of secondary phase particles will induce a pinning effect that will be added to the solute drag phenomenon to prevent grain growth.

Concerning the influence of microstructure on optical properties, two behaviours have to be considered depending on whether secondary phase particles are present or not. For AZ150 and AZ280, XRD measurements indicate that no secondary phase particles are formed. This suggests that light scattering only depends on grain size and porosity (Eqs. (1)–(3)). This assumption implies that the segregation of Zr^{4+} cations along grain boundaries does not contribute to light scattering. This has been demonstrated by Bernard-Granger et al.[9,10] who succeeded in obtaining transparent PCA doped with Mg^{2+}, Ti^{4+} and Ca^{2+}/Ti^{4+}. In their studies, the doping cations only segregated

along grain boundaries without secondary phase particle formation and the RIT measurements in the visible range presented a good correlation with the theoretical curves obtained with the Apetz model (Eqs. (1) and (2)). That is why for AZ150 and AZ280, only scattering due to porosity and from grain boundaries is considered.

Transparency requires no porosity or such a limited amount that it could not be measured by the classical Archimede method. However, as measured grain sizes are between 300 nm and 3 μm and no secondary phase particles are formed on AZ150 and AZ280 samples, it is possible to compare our results with the theoretical model developed by Apetz (Eqs. (1) and (2)). Theoretical curves (Fig. 6) were calculated for a 100 nm pore size as it is the largest pore size which can be observed by TEM (Fig. 4). Moreover, this corresponds to the critical pore size.[14]

As the grain size is larger at $1300\,°C$ than $1280\,°C$ (Fig. 3), this means that the lower transparency obtained at $1280\,°C$ compared to $1300\,°C$ can be explained by greater porosity (Fig. 6). Thus, at $1280\,°C$, the densification is not yet complete and some critical porosity (>50 nm[14]) is still present, affecting the RITs$_{640nm}$. Higher RITs$_{640nm}$ are thus obtained at $1300\,°C$ for all amounts of doping agent (Fig. 2). At this temperature, the densification is sufficient to limit the presence of pores with a limited grain growth. Light scattering by both pores and grain boundaries is then limited.[11] Moreover, for a given temperature, the RITs$_{640nm}$ of Zr-doped samples decrease with the increase in amount of doping agent (Fig. 2). This decrease is due to the increase in porosity, as shown in Fig. 6, indicating different densification behaviours.

For AZ570, m-ZrO$_2$ particles are found within the alumina matrix (Figs. 4(c) and 5) which will also contribute to light scattering (Eq. (3)).

3.1.3. Sintering

As discussed above, samples doped with different amounts of Zr^{4+} cations may have different sintering behaviours. The densification rates of the different powders sintered at $T_f = 1280\,°C$ are shown in Fig. 7 and are compared with the pure alumina freeze-dried powder sintered using the same sintering cycle.
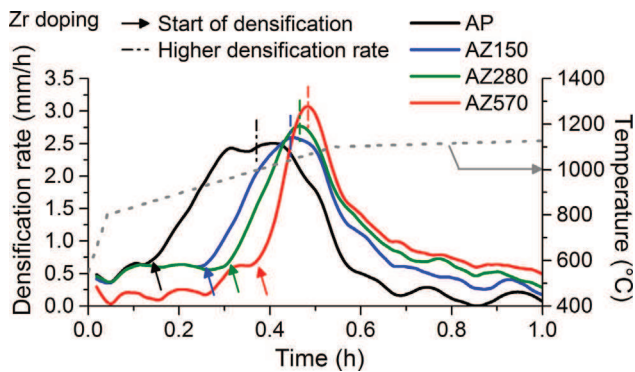
Fig. 7. Densification rate of freeze-dried alumina powders pure or doped with different amounts of Zr^{4+} cations.

As can be seen from Fig. 7, doping alumina powders with Zr^{4+} cations delays the densification at higher temperatures whatever the amount of doping agent. Moreover, increasing the doping agent amount also tends to delay the densification at higher temperatures even if this effect is less pronounced. Indeed, the densification of AP starts at 850 °C, compared to 930, 960 and 1000 °C for AZ150, AZ280, and AZ570, respectively. The higher densification rates are obtained at 1050, 1060 and 1070 °C for AZ150, AZ280, and AZ570, respectively, compared to 1000 °C for pure alumina samples (AP).

Segregated Zr^{4+} cations along grain boundaries favour the presence of aluminium vacancies at their vicinity to preserve electrical neutrality. Consequently, diffusion mechanisms of Al^{3+} cations along these grain boundaries should be favoured. Some authors[28–31] have proved that the densification of α-alumina by SPS is controlled by grain boundary diffusion but the rate controlling species are not known for certain. Currently, no studies have been able to ascertain whether aluminium grain boundary diffusion is greater or smaller than oxygen grain boundary diffusion.[32] This means that the promotion of Al^{3+} cations diffusion mechanisms may not improve the densification of α-alumina if the rate controlling species are O^{2-} anions. In our study, segregated Zr^{4+} cations at grain boundaries delay the densification at higher temperatures. According to Yoshida,[2] the substitution of an Al^{3+} cation by a Zr^{4+} cation increases the ionic bonding strength between Al^{3+} cations and O^{2-} anions. It thus slows down the grain boundary and lattice diffusions of both species (grain boundaries are the origin of diffusion in both cases). As a result, the densification is delayed at higher temperatures.

Finally, as the densification of samples doped with a greater amount of Zr^{4+} cations is more difficult (slight delay at higher temperatures), this could explain why these samples show more porosity after sintering and thus reduce transparency.

3.2. La-doped alumina

3.2.1. Optical properties

La-doped powders were sintered at different T_f: 1230, 1250, 1280, 1300 and 1330 °C. The highest $RITs_{640nm}$ were obtained at $T_f = 1250$, 1280 and 1300 °C and these results are presented in Fig. 8.
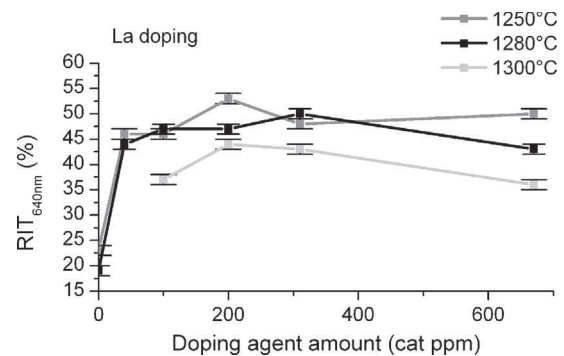

Fig. 8. $RITs_{640nm}$ of La-doped alumina samples sintered at $T_f = 1250$ °C, 1280 °C and 1300 °C for different amounts of doping agent.
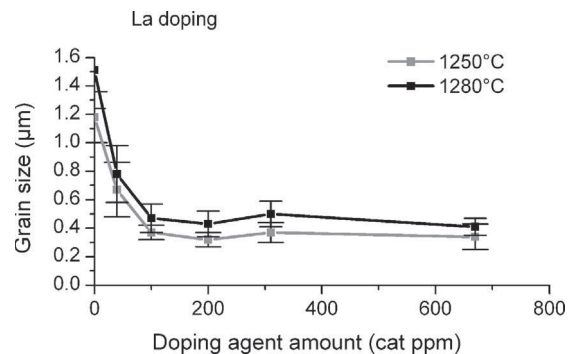

Fig. 9. Average grain sizes of La-doped alumina samples sintered at $T_f = 1250$ °C and 1280 °C for different amounts of doping agent.

Doping with La^{3+} cations enables an increase in the RIT_{640nm} of alumina samples due to a reduced grain size (Fig. 9). Moreover, $RITs_{640nm}$ of samples sintered at 1250 and 1280 °C are very similar. This is in good agreement with work by Roussel et al.[33] who found that doping PCA with La^{3+} cations enables high transparency to be obtained over a large range of sintering temperatures.

Interestingly, adding La^{3+} cations above 100 cat ppm has no additional effect on the grain size which remains constant at around 0.35 μm and 0.45 μm, at 1250 °C and 1280 °C, respectively. As γ_G, the light scattering coefficient by grain boundaries, depends only on grain size (Eq. (2)), this means that the differences between the $RITs_{640nm}$ of samples sintered at the same temperature are due to either porosity (γ_P) or secondary phase particles (γ_{dop}) (Eqs. (1)–(3)). TEM observations could help us clarify this point.

3.2.2. TEM analysis

The atomic number of La ($Z = 57$) is higher than that of Al ($Z = 13$). HAADF observations can thus be performed to indicate the presence of La^{3+} cations within an alumina matrix. Such observations were performed with EDX spectroscopy on samples doped with different amounts of La^{3+} cation. They revealed that no La^{3+} cations are located within alumina grains (Fig. 10(a)). Lanthanum segregation is found along grain boundaries (Fig. 10(c)). Moreover, secondary phase particles are only formed for the highest La-doped samples AL310 and AL670 (Fig. 10(b and c)). This means that the La^{3+} grain boundary
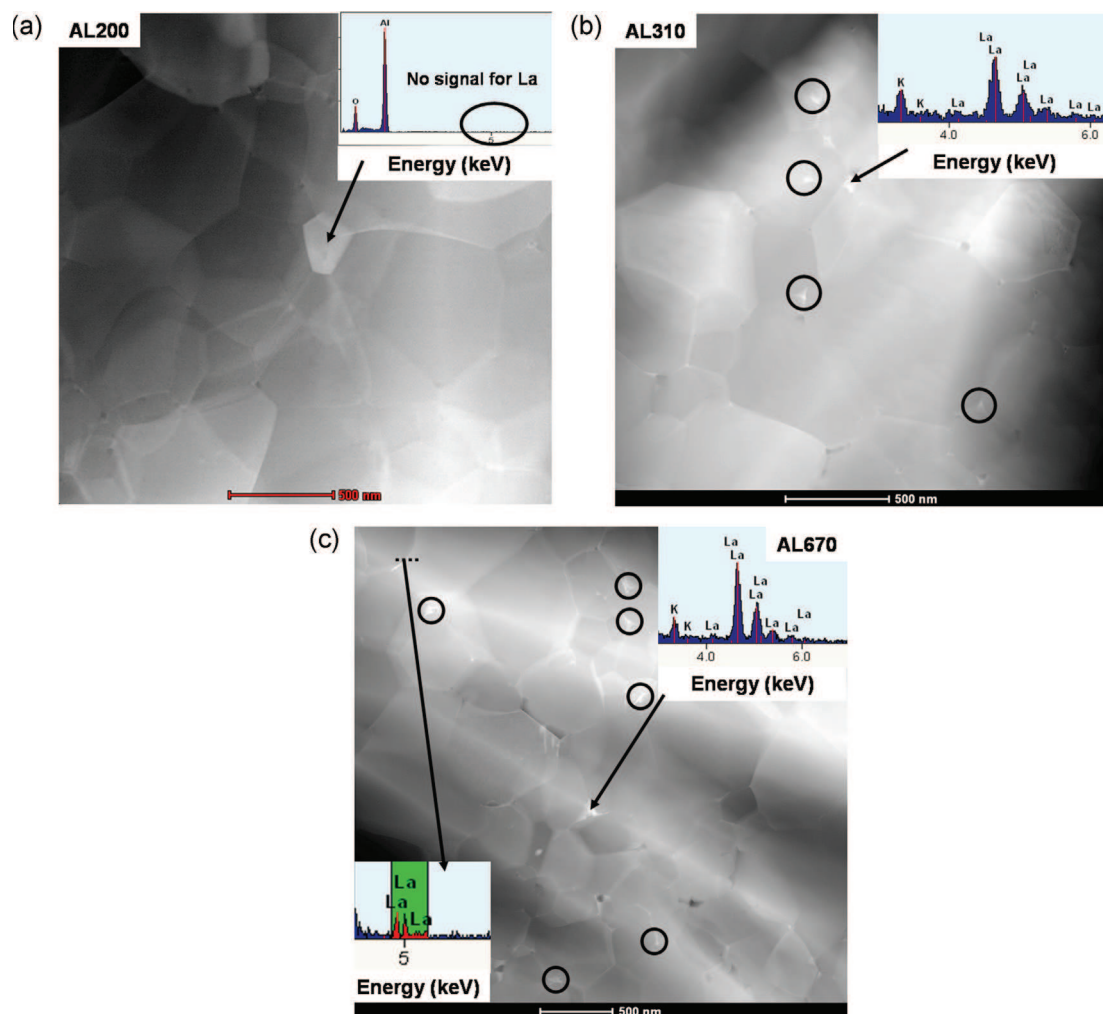
Fig. 10. HAADF observations and EDX spectroscopy of (a) AL200, (b) AL310, and (c) AL670 samples. Arrows indicate the EDX analysis point.

Table 2
Atomic ratios of the elements present within a lanthanum secondary phase particle.

Element	Atomic ratio (%)
Carbon	1.29 ± 0.06
Oxygen	56.36 ± 0.33
Aluminium	37.53 ± 0.25
Chlorine	2.83 ± 0.07
Lanthanum	1.97 ± 0.18

solubility is between 200 and 310 cat ppm La for a 400 nm Al_2O_3 grain size.

EDX spectroscopy within a secondary phase particle reveals the presence of lanthanum, aluminium, oxygen and chlorine. Chlorine is due to the lanthanum chloride salt used as the precursor for doping. The atomic ratios of these different elements are given in Table 2. For this estimation, the peaks were first identified before subtracting the background of the spectrum. Then, the Cliff–Lorimer method was used to correlate the intensity of the signal with element concentration. Finally, it was assumed that the summation of all calculated concentrations is equal to 1. Based on these results, the secondary phase is supposed to be a

β-alumina $LaAl_{11}O_{18}$ structure as the atomic ratios are close to those in such a structure (3.4% La, 36.6% Al and 60% O). It is also in agreement with XRD results obtained on AL670 (Fig. 5).

As for Zr^{4+} cations, the presence of La^{3+} cations at grain boundaries hinders diffusion across these boundaries. Moreover, the solute drag effect prevents their mobility.[27] From 0 to 100 cat ppm, those phenomena reduce the grain boundary mobility all the more as the amount of doping agent increases. Above 100 cat ppm, grain size is constant (Fig. 9). This suggests that the diffusion across grain boundaries is blocked and that neither an addition of segregated cations nor the formation of secondary phase particles will further inhibit grain growth.

Concerning the influence of microstructure on optical properties when no secondary phase particles are formed (for the samples AL40, AL100 and AL200), only the degree of light scattering due to grain size and porosity has to be considered. The results are thus compared with the theoretical model developed by Apetz (Eqs. (1) and (2)). Theoretical curves (Fig. 11) were therefore calculated for a 100 nm pore size as it is the largest pore size observed by TEM (Fig. 10).

Increasing the amount of lanthanum reduces the grain size but at the same time it does not allow a better densification to
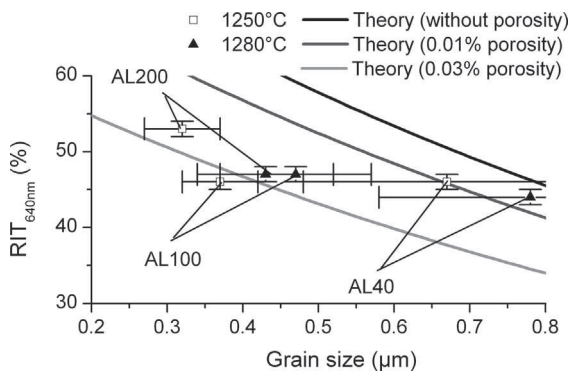
Fig. 11. Comparison of RITs$_{640nm}$ of AL40, AL100 and AL200 samples sintered at $T_f = 1250\,°C$ and $1280\,°C$ with theoretical models ($\lambda_0 = 640$ nm, $D = 0.88$ mm, $\phi_p = 100$ nm).
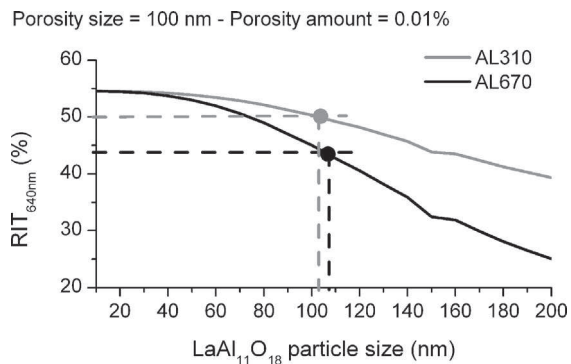

Fig. 12. Theoretical curves of RIT$_{640nm}$ versus the diameter of LaAl$_{11}$O$_{18}$ particles for different amounts of doping agent ($\lambda_0 = 640$ nm, $D = 0.88$ mm, $\phi_G = 450$ nm, $\phi_p = 100$ nm, $p = 0.01\%$).

be obtained because the porosity is greater (0.03%). The study of the sintering behaviour of La-doped samples will thus be discussed in the next section.

For samples doped with a larger amount of La^{3+} cations (AL310 and AL670), β-alumina LaAl$_{11}$O$_{18}$ particles are observed (Fig. 10(b and c)). Due to its different refractive index compared to alumina (about 1.78[34] and 1.76 for LaAl$_{11}$O$_{18}$ and α-alumina, respectively), the LaAl$_{11}$O$_{18}$ phase can induce light scattering (Eq. (3)). For example, at $1280\,°C$, the RIT$_{640nm}$ value decreases from $50 \pm 1\%$ to $43 \pm 1\%$ between AL310 and AL670 samples. This decrease occurs without grain growth. The contribution of the secondary phase particles to this decrease is evaluated in Fig. 12. Theoretical curves were calculated for a grain size of 450 nm as it corresponds to that obtained for samples sintered at $T_f = 1280\,°C$. The pore size was fixed at 100 nm as it is the largest pore size observed by TEM. Moreover, the largest secondary phase particles observed by TEM are around 100 nm for both samples. According to the Apetz model, the residual porosity should be around 0.01%, which is lower than the one found on less doped samples (0.03%). Alvarez-Clemares et al.[35] have shown that cerium oxide secondary phase particles are located at grain boundaries and triple points within PCA, closing the pores usually located at these positions. We can thus assume an equivalent behaviour of β-alumina particles which
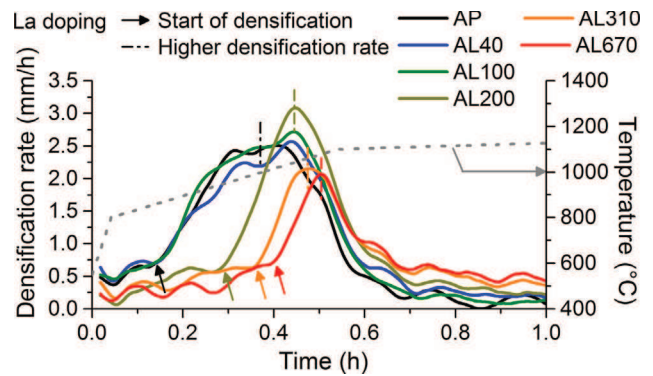

Fig. 13. Densification rate of freeze-dried alumina powders, pure or doped with different amounts of La^{3+} cations.

were also located at triple points. That is why the porosity is lower for samples having secondary phase particles.

3.2.3. Sintering

Freeze-dried powders doped with different amounts of La^{3+} cations were sintered by SPS at $T_f = 1280\,°C$. The densification rates of the different powders are shown in Fig. 13.

As can be seen from Fig. 13, the densification behaviour of slightly doped samples (below 100 cat ppm) is similar to that of undoped samples. We can thus initially assume that the amount of La^{3+} cations is lower than their bulk solubility limit (no segregated cations along the grain boundaries) since densification is controlled by grain boundary diffusion mechanisms. Nevertheless, Fig. 9 shows that the grain size is already decreasing for doping amounts as low as 40 cat ppm, suggesting that the doping agent is already segregated at the grain boundaries and is active in limiting grain growth. Therefore, it is as though the lanthanum bulk solubility limit is below 40 cat ppm, as calculated by Galmarini,[4] even if below 100 cat ppm segregated La^{3+} cations have no detectable effects on the densification behaviour of alumina samples. Above 100 cat ppm, the densification of La-doped samples is delayed at higher temperatures. The densification of AP starts at $850\,°C$, compared to 940, 990 and $1010\,°C$ for AL200, AL310, and AL670, respectively. The higher densification rates are obtained at 1050, 1070 and $1090\,°C$ for AL200, AL310 and AL670 compared to $1000\,°C$ for pure alumina samples (AP). This is due to the larger amount of La^{3+} cations along grain boundaries or at triple points that hinder the diffusion mechanisms responsible for densification. However, too many segregated La^{3+} cations may hinder porosity reduction at the end of sintering thus explaining why AL40 and AL100 have a similar densification rate profile but the porosity after sintering is found to be greater for AL100 samples (Fig. 11).

3.3. Optimised Zr and La doping conditions

Obtaining transparent PCA samples is all about finding the best compromise between grain size, porosity and amount of doping agent. The presence of secondary phase particles or significant segregation along grain boundaries has to be avoided as either clearly decrease transparency (Fig. 12). A small amount of doping agent is thus preferred because it enables a reduction

in the grain size without secondary phase formation. Moreover, samples doped with different agents of different nature and/or amount could lead to similar RIT_{640nm} values providing that the sintering cycle is adapted. For example, AZ280 and AL40 both lead to $RIT_{640nm} \sim 44 \pm 1\%$ but their sintering temperatures are different ($T_f = 1300\,°C$ and $1280\,°C$ for AZ280 and AL40, respectively).

Finally, the optimised cation amounts for transparency are found to be 150 and 200 cat ppm for Zr- and La-doped samples, respectively. The highest RIT_{640nm} of $53 \pm 1\%$ obtained in this study for AL200 samples sintered at $T_f = 1250\,°C$ is equivalent to the one of Stuer for 225 cat ppm La-doped alumina[7] also obtained with freeze-dried powders. Nevertheless, this value also corresponds to the one obtained in our previous study[24] on the green body processing optimisation for *pure* α-alumina before sintering by SPS. Thus, combining the beneficial effects of the green body particle packing optimisation and the addition of the good amount of grain growth inhibitor in a finer alumina powder will again improve the optical properties of α-alumina sintered by SPS up to 71% RIT_{640nm} as demonstrated in Ref. 33.

4. Conclusions

The effect of amount of doping agent on microstructure and optical properties of Zr- and La-doped alumina has been investigated. Both Zr^{4+} and La^{3+} are grain growth inhibitors and thus enable the optical properties of spark plasma sintered alumina to be increased. Moreover, both doping cations are insoluble (or nearly) in the α-alumina lattice and disturb the grain boundary diffusion. Densification is thus delayed and occurs at higher temperatures.

Zr^{4+} cations segregate at grain boundaries for amounts of doping agent as high as 280 cat ppm with a grain size of 450 nm. At 570 cat ppm, a few particles of monoclinic zirconia are formed. The optimised amount of Zr^{4+} cations to obtain transparent PCA is around 150 cat ppm even if the grain size is not the finest, because no secondary phase particles are formed and the densification is easier than for higher doping amounts (slight delay towards higher temperatures). A maximum RIT_{640nm} of $48 \pm 1\%$ is found for sintering at $T_f = 1300\,°C$.

La^{3+} cations first segregate at grain boundaries before forming β-alumina $LaAl_{11}O_{18}$ particles at 310 cat ppm La for a grain size of 450 nm. Nevertheless, 100 cat ppm of segregated La^{3+} cations are sufficient to block the diffusion path across grain boundaries. As a result, the grain size of La-doped samples is constant for higher than 100 cat ppm La^{3+}.

For both doping agents, the reduction in optical properties (transparency) is attributed to an increase in the porosity when no secondary phase particles are formed. After the formation of a secondary phase, those particles contribute to light scattering; the more particles there are the more scattering is observed.

Finally, the highest RIT_{640nm} of $53 \pm 1\%$ is obtained when doping with 200 cat ppm of La, though it can still be improved by optimising the green body processing.[33]

References

1. Yoshida H, Ikuhara Y, Sakuma T. Vacancy effect of dopant cation on the high-temperature creep resistance in polycrystalline Al_2O_3. *Mater Sci Eng A* 2001;**319–321**:843–8.
2. Yoshida H, Ikuhara Y, Sakuma T. Grain boundary electronic structure related to the high-temperature creep resistance in polycrystalline Al_2O_3. *Acta Mater* 2002;**50**(11):2955–66.
3. Yoshida H, Hashimoto S, Yamamoto T. Dopant effect on grain boundary diffusivity in polycrystalline alumina. *Acta Mater* 2005;**53**(2):433–40.
4. Galmarini S, Aschauer U, Tewari A, Aman Y, Van Gestel C, Bowen P. Atomistic modeling of dopant segregation in α-alumina ceramics: coverage dependent energy of segregation and nominal dopant solubility. *J Eur Ceram Soc* 2011;**31**(15):2839–52.
5. Swiatnicki W, Lartigue-Korinek S, Laval JY. Grain boundary structure and intergranular segregation in Al_2O_3. *Acta Metal Mater* 1995;**43**(2):795–805.
6. Voytovych R, MacLaren I, Gülgün M, Cannon R, Rühle M. The effect of yttrium on densification and grain growth in α-alumina. *Acta Mater* 2002;**50**(13):3453–63.
7. Stuer M, Zhao Z, Aschauer U, Bowen P. Transparent polycrystalline alumina using spark plasma sintering: effect of Mg, Y and La doping. *J Eur Ceram Soc* 2010;**30**(6):1335–43.
8. Krell A, Blank P, Ma H, Hutzler T, Van Bruggen MPB, Apetz R. Transparent sintered corundum with high hardness and strength. *J Am Ceram Soc* 2003;**86**(1):12–8.
9. Bernard-Granger G, Guizard C. Influence of MgO or TiO_2 doping on the sintering path and on the optical properties of a submicronic alumina material. *Scr Mater* 2007;**56**(11):983–6.
10. Bernard-Granger G, Guizard C, Addad A. Influence of Co-doping on the sintering path and on the optical properties of a submicronic alumina material. *J Am Ceram Soc* 2008;**91**(5):1703–6.
11. Roussel N, Lallemant L, Durand B, Guillemet S, Chane Ching JY, Fantozzi G, et al. Effects of the nature of the doping salt and of the thermal pretreatment and sintering temperature on spark plasma sintering of transparent alumina. *Ceram Int* 2011;**37**(8):3565–73.
12. Stuer M, Zhao Z, Bowen P. Freeze granulation: powder processing for transparent alumina applications. *J Eur Ceram Soc* 2012;**32**(11):2899–908.
13. Apetz R, Van Bruggen MPB. Transparent alumina: a light-scattering model. *J Am Ceram Soc* 2003;**86**(3):480–6.
14. Stuer M, Bowen P, Cantoni M, Pecharroman C, Zhao Z. Nanopore characterization, optical modeling of transparent polycrystalline alumina. *Adv Funct Mater* 2012;**22**:2303–9.
15. Kim BN, Hiraga K, Morita K, Yoshida H, Kagawa Y. Light scattering in MgO-doped alumina fabricated by spark plasma sintering. *Acta Mater* 2010;**58**(13):4527–35.
16. Pecharroman C, Mata-Osoro G, Daaz LA, Torrecillas R, Moya JS. On the transparency of nanostructured alumina: Rayleigh-Gans model for anisotropic spheres. *Opt Express* 2009;**17**(8):6899–912.
17. Cho J, Wang CM, Chan HM, Rickman JM, Harmer MP. A study of grain-boundary structure in rare-earth doped aluminas using an EBSD technique. *J Mater Sci* 2002;**37**(1):59–64.
18. Bruley J, Cho J, Chan HM, Harmer MP, Rickman JM. Scanning transmission electron microscopy analysis of grain boundaries in creep-resistant

yttrium- and lanthanum-doped alumina microstructures. *J Am Ceram Soc* 1999;**82**(10):2865–70.

19. Wang CM, Cargill GS, Chan HM, Harmer MP. Structure of Y and Zr segregated grain boundaries in alumina. *Interface Sci* 2000;**8**(2):243–55.

20. Shannon R. Revised effective ionic radii and systematic studies of interatomic distances in halides and chalcogenides. *Acta Crystallogr A* 1976;**32**:751–67.

21. Djuricic B, Pickering S, Glaude P, McGarry D, Tambuyser P. Thermal stability of transition phases in zirconia-doped alumina. *J Mater Sci* 1997;**32**(3):589–601.

22. Thompson AM, Soni KK, Chan HM, Harmer MP, Williams D, Chabala J, et al. Dopant distributions in rare-earth-doped alumina. *J Am Ceram Soc* 1997;**80**(2):373–6.

23. Fang J, Thompson AM, Martin PH, Helen MC. Effect of yttrium and lanthanum on the final-stage sintering behavior of ultrahigh-purity alumina. *J Am Ceram Soc* 1997;**80**(8):2005–12.

24. Lallemant L, Fantozzi G, Garnier V, Bonnefont G. Transparent polycrystalline alumina obtained by SPS: green bodies processing effect. *J Eur Ceram Soc* 2012;**32**(11):2909–15.

25. Kim BN, Hiraga K, Morita K, Yoshida H. Spark plasma sintering of transparent alumina. *Scr Mater* 2007;**57**(7):607–10.

26. Kim BN, Hiraga K, Morita K, Yoshida H. Effects of heating rate on microstructure and transparency of spark-plasma-sintered alumina. *J Eur Ceram Soc* 2009;**29**(2):323–7.

27. Kang SJL. *Sintering densification, grain growth & microstructure*. Butterworth-Heinemann; 2005.

28. Langer J, Hoffmann MJ, Guillon O. Direct comparison between hot pressing and electric field-assisted sintering of submicron alumina. *Acta Mater* 2009;**57**(18):5454–65.

29. Santanach JG, Weibel A, Estournes C, Yang Q, Laurent C, Peigney A. Spark plasma sintering of alumina: study of parameters, formal sintering analysis and hypotheses on the mechanism(s) involved in densification and grain growth. *Acta Mater* 2011;**59**(4):1400–8.

30. Aman Y, Garnier V, Djurado E. Spark plasma sintering kinetics of pure α-alumina. *J Am Ceram Soc* 2011;**94**(9):2825–33.

31. Demuynck M, Erauw JP, Van der Biest O, Delannay F, Cambier F. Densification of alumina by SPS and HP: a comparative study. *J Eur Ceram Soc* 2012;**32**(9):1957–64.

32. Heuer A. Oxygen and aluminum diffusion in α-Al_2O_3: how much do we really understand? *J Eur Ceram Soc* 2008;**28**:1495–507.

33. Roussel N, Lallemant L, Chane Ching JY, Guillemet S, Durand B, Garnier V, et al. Highly dense: transparent α-Al_2O_3 ceramics from ultrafine nanoparticles via a standard SPS sintering. *J Am Ceram Soc* 2013;**96**(4):1039–42.

34. Yamashita I, Tsukuma K, Kusunose T. Translucent Al_2O_3/$LaAl_{11}O_{18}$ composite. *J Am Ceram Soc* 2009;**92**(9):2136–8.

35. Alvarez-Clemares I, Mata-Osoro G, Fernandez A, Lopez-Esteban S, Pecharroman C, Torrecillas R, et al. Ceria doped alumina by spark plasma sintering for optical applications. *J Eur Ceram Soc* 2012;**32**(11):2917–24.